

## New Constraints on Exotic Spin-Spin-Velocity-Dependent Interactions with Solid-State Quantum Sensors

Yue Huang,<sup>1,2</sup> Hang Liang,<sup>1,2</sup> Man Jiao<sup>1,2,3,\*</sup>, Pei Yu,<sup>1,2</sup> Xiangyu Ye,<sup>1,2</sup> Yijin Xie<sup>1,2,3</sup>, Yi-Fu Cai<sup>1,2,4,5</sup>, Chang-Kui Duan<sup>1,2,6</sup>,  
Ya Wang<sup>1,2,6</sup>, Xing Rong,<sup>1,2,6,†</sup> and Jiangfeng Du<sup>1,2,3,6,‡</sup>

<sup>1</sup>CAS Key Laboratory of Microscale Magnetic Resonance and School of Physical Sciences,

University of Science and Technology of China, Hefei 230026, China

<sup>2</sup>CAS Center for Excellence in Quantum Information and Quantum Physics,

University of Science and Technology of China, Hefei 230026, China

<sup>3</sup>Institute of Quantum Sensing and School of Physics, Zhejiang University, Hangzhou 310027, China

<sup>4</sup>CAS Key Laboratory for Researches in Galaxies and Cosmology, School of Astronomy and Space Science,

University of Science and Technology of China, Hefei, Anhui 230026, China

<sup>5</sup>Department of Astronomy, School of Physical Sciences, University of Science and Technology of China, Hefei, Anhui 230026, China

<sup>6</sup>Hefei National Laboratory, University of Science and Technology of China, Hefei 230088, China



(Received 8 September 2023; revised 6 February 2024; accepted 26 March 2024; published 30 April 2024)

We report new experimental results on exotic spin-spin-velocity-dependent interactions between electron spins. We designed an elaborate setup that is equipped with two nitrogen-vacancy (NV) ensembles in diamonds. One of the NV ensembles serves as the spin source, while the other functions as the spin sensor. By coherently manipulating the quantum states of two NV ensembles and their relative velocity at the micrometer scale, we are able to scrutinize exotic spin-spin-velocity-dependent interactions at short force ranges. For a T-violating interaction,  $V_6$ , new limits on the corresponding coupling coefficient,  $f_6$ , have been established for the force range shorter than 1 cm. For a P,T-violating interaction,  $V_{14}$ , new constraints on the corresponding coupling coefficient,  $f_{14}$ , have been obtained for the force range shorter than 1 km.

DOI: [10.1103/PhysRevLett.132.180801](https://doi.org/10.1103/PhysRevLett.132.180801)

Ultralight new bosons ( $m_b \lesssim 1 \text{ eV}/c^2$ ) [1] beyond the standard model are proposed to explain mysteries of modern physics, such as strong  $CP$  problem [2–4], the hierarchy problem [5], and the composition of dark matter [6]. It is predicted that these hypothetical bosons, including axions [7], familons [8], paraphotons [9],  $Z'$  bosons [10], etc., can serve as mediators of exotic interactions between fermions [11,12]. Such spin-0 or spin-1 boson exchanges within a Lorentz-invariant quantum field theory can be categorized into 15 exotic spin-dependent interactions, which enable methodical exploration with astrophysical and laboratory searches [12,13].

With recent advances in precision measurement, spin based sensors play a vital role in tabletop experiments searching for the exotic spin-dependent interactions [14], such as the ion trap [15], atomic magnetometer [16–19], scanning probe microscope [20], nitrogen-vacancy (NV) centers in diamond [21–24], and polarized torsion pendulum [25,26]. Exotic spin-spin-velocity-dependent

interactions (SSVDIs) can be mediated by spin-1 bosons including the new massless paraxial photons and light  $Z'$  bosons [12]. In contrast to interactions introduced by spin-0 bosons, interactions mediated by new spin-1 bosons can avoid astrophysical constraints due to potential loopholes [12,27], making direct laboratory searching important and necessary. While static exotic spin-spin interactions have been strictly constrained over a broad range of distance scales [21,25,26,28–30], the investigation of SSVDIs is less extensive, especially in the force range below 1 cm [16,31]. The experimental search at short force ranges remains unexplored due to the challenges in coherently steering quantum states of electron spins, high precision magnetic sensing, and spatial position modulation at micrometer scale.

In this Letter, we experimentally investigated SSVDIs between polarized electrons utilizing two individual ensemble-NV diamonds. One type of the SSVDIs whose potential follows the notation in Ref. [12] can be given as

$$V_6 = -f_6 \frac{\hbar^2}{4\pi m_e c} [(\hat{\sigma}_1 \cdot \vec{v})(\hat{\sigma}_2 \cdot \hat{r}) + (\hat{\sigma}_1 \cdot \hat{r})(\hat{\sigma}_2 \cdot \vec{v})] \left( \frac{1}{\lambda r} + \frac{1}{r^2} \right) e^{-r/\lambda}, \quad (1)$$

Published by the American Physical Society under the terms of the [Creative Commons Attribution 4.0 International license](https://creativecommons.org/licenses/by/4.0/). Further distribution of this work must maintain attribution to the author(s) and the published article's title, journal citation, and DOI. Funded by SCOAP<sup>3</sup>.

where  $f_6$  is the dimensionless coupling coefficient, and  $\hat{\sigma}_1$  and  $\hat{\sigma}_2$  are the unit spin vectors of the two interacting fermions, respectively.  $\mathbf{v}$  is the relative velocity between them,  $r = |\mathbf{r}|$  is the displacement, and  $\hat{r}$  is the unit displacement vector.  $\hbar$  is the reduced Planck's constant,  $c$  is the speed of light in vacuum, and  $m_e$  is the mass of the electron.  $\lambda = \hbar/m_b c$  is the interaction range determined by the mass of the mediated new boson  $m_b$ . The SSVDI can be induced by the exchange of virtual  $Z'$  bosons [12], which are motivated by various theoretical scenarios of beyond-the-standard-model physics, and are candidates for dark matter [32]. Laboratory searching for the SSVDI offers a promising avenue to further our understanding of  $Z'$  bosons' fundamental physics. The exotic interaction can be characterized as an effective magnetic field acting on NV electron spins. It can be described as

$$B_6 = -f_6 \frac{\hbar}{2\pi m_e \gamma c} [(\hat{\sigma}_1 \cdot \mathbf{v})(\hat{\sigma}_2 \cdot \hat{r}) + (\hat{\sigma}_1 \cdot \hat{r})(\hat{\sigma}_2 \cdot \mathbf{v})] \left( \frac{1}{\lambda r} + \frac{1}{r^2} \right) e^{-r/\lambda}, \quad (2)$$

where  $\gamma$  is the gyromagnetic ratio of the electron spin. In this work, we utilized an NV ensemble as a magnetometer to search for the possible magnetic field due to the SSVDI from another NV ensemble, which acts as a polarized electron spin source. Compared with previously used electron spin sources such as  $\text{SmCo}_5$  magnets [16], the electron spin states of NV ensembles can be modulated instantaneously and efficiently via optical and microwave pulses. Moreover, the small geometry size of the ensemble-NV diamonds enables close proximity between the spin sensor and spin source, which is essential for detecting exotic spin-dependent interactions at short force ranges.

The geometric schematic of our setup is shown in Fig. 1(a). We used two  $660 \times 661 \times 574 \mu\text{m}^3$  diamond crystals (labeled with Diamond I and II in Fig. 1) with  $\langle 100 \rangle$  oriented surfaces. NV centers with a concentration being 14 (22) ppm were doped within a thin layer  $h_1$  ( $h_2$ ) = 23  $\mu\text{m}$  at the Diamond I (II) surface, and were utilized as the spin sensor (source) for SSVDIs, respectively. The spin source was placed above the spin sensor, where the distance between the two diamonds was  $d$  being 18.5  $\mu\text{m}$ . To separately manipulate and read out the spin states of the spin sensor and the spin source, we constructed two sets of laser and fluorescence collection channels. The spin sensor was illuminated by a 532-nm laser with a beam diameter of about 40  $\mu\text{m}$  via the flank of the diamond. The red fluorescence emitted from the spin sensor was collected via a compound parabolic concentrator below. The other green laser was sent through an objective above to excite the spin source with a spot radius  $R$  being 52  $\mu\text{m}$ . The fluorescence from the spin source was collected by the same objective. A 500-nm silver layer was fabricated on Diamond II to isolate the two laser beams as well as

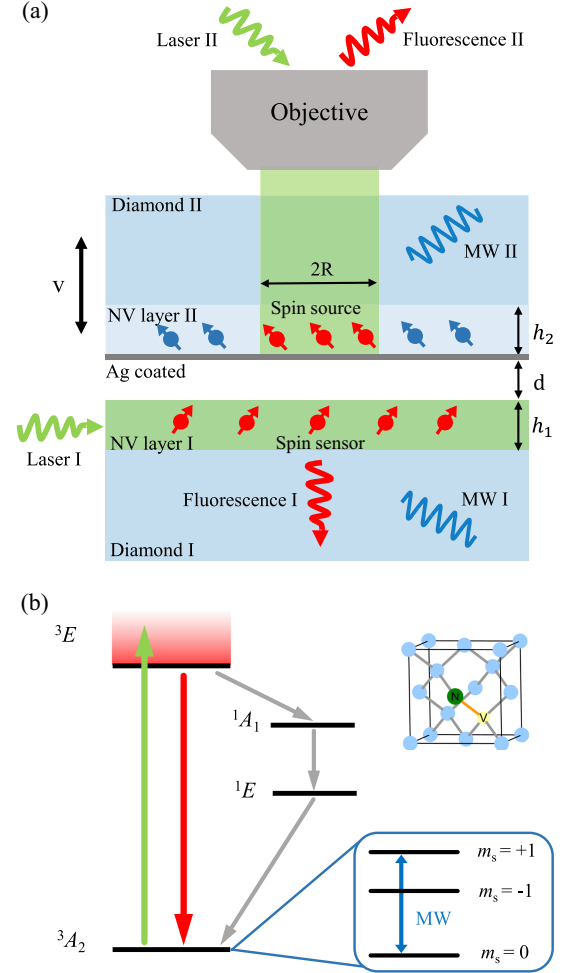


FIG. 1. (a) Schematic experimental setup. The spin sensor is a thin NV layer on Diamond I. The spin source is another thin NV layer on Diamond II. The laser and microwave applied on the spin sensor (source) are labeled as Laser I (II) and MW I (II), respectively. There was a silver layer isolating the two optically detected systems. The spin source was modulated to vibrate perpendicularly to the diamond surface. (b) Energy-level diagram and atomic structure of NV center in diamond. NV electronic spin states can be optically initialized and read out.

fluorescence from two NV layers. The sensing area of the spin sensor and the polarized region of the spin source were monitored by an upper camera according to fluorescence images (see Supplemental Material for details [33]). To investigate SSVDIs, the spin source was modulated by a piezoelectric Bender to vibrate at  $\mathbf{v}$  with frequency  $f_{\text{vib}} = 1.337 \text{ kHz}$ .

As shown in Fig. 1(b), NV ground state is an electron spin triplet state with three spin states  $|m_s = 0\rangle$  and  $|m_s = \pm 1\rangle$  [37]. A static magnetic field  $B_0$  being 94 gauss was applied along the NV symmetry axis of the spin sensor to separate  $|m_s = \pm 1\rangle$  spin states. We positioned the two diamonds with a relative angle of  $54^\circ$  rotated along the vertical direction, such that the projection of the bias magnetic field  $B_0$  onto the NV axis differed for each

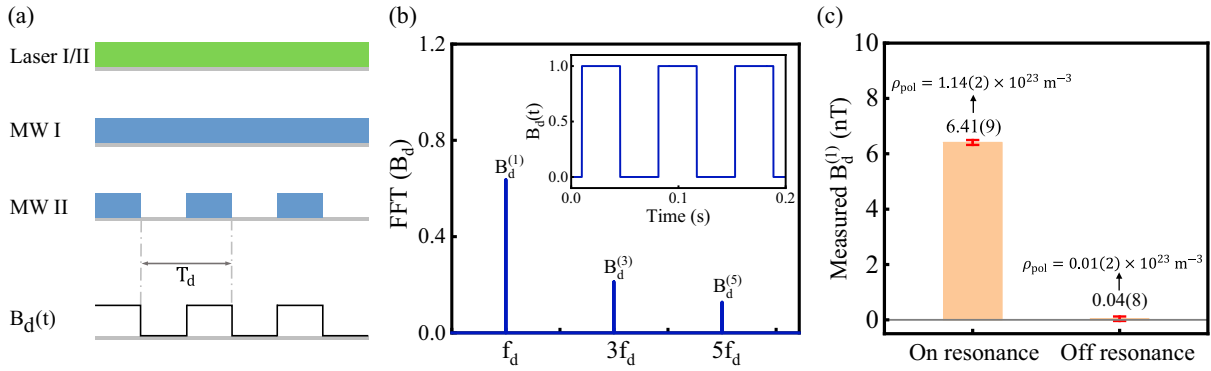


FIG. 2. Measurement of the polarized spin density of the spin source. (a) The laser and the microwave sequences and the time evolution of the magnetic dipole field  $B_d$ .  $T_d = 1/f_d$ . (b) Fourier transformation spectrum of  $B_d$ . Inset: square-wave signal of  $B_d$  in time domain. (c) Experimental results of the measured magnetic dipole fields and the measured polarized spin densities under on-resonance and off-resonance conditions.

sample. It resulted in the difference between the  $|m_s = 0\rangle \rightarrow |m_s = +1\rangle$  transition frequencies of the two NV ensembles, which enabled us to control them independently via microwaves of two distinct frequencies (see Supplemental Material for details [33]).

The spin sensor is an ensemble-NV diamond magnetometer. A typical continuous-wave method was carried out with the  $|m_s = 0\rangle \rightarrow |m_s = +1\rangle$  transition of the sensor, wherein laser and microwave field were continuously applied [38,39]. We applied frequency modulation to the microwave on the spin sensor, encoding the magnetic-field information in a band around the modulation frequency. The laser fluctuation was also recorded for noise cancellation. The magnetic sensitivity of the ensemble-NV diamond magnetometer is  $2 \text{ nT}/\sqrt{\text{Hz}}$  within the frequency range from 1 to 2 kHz (see Supplemental Material for details [33]).

First, the polarized spin density of the spin source was obtained by measuring the magnetic dipole-dipole interaction between the spin sensor and the spin source. Figure 2(a) shows schematically the experimental laser and microwave sequences. The magnetic polarization of the spin source was modulated by periodically switching MW II with 50% duty cycle at frequency being 14 Hz. When the laser continuously pumped the spin source to  $|m_s = 0\rangle$ , nonzero magnetic polarization of the electron spin can be realized with the resonant microwave. Since the polarization changes fast during the switching process of MW II, the magnetic field  $B_d$  sensed by the spin sensor can be characterized as a square wave (see Supplemental Material for details [33]). Thus, it can be decomposed into a series of odd sinusoidal harmonics:

$$B_d = -\frac{\mu_0 \gamma \hbar}{8\pi} \frac{1}{V_I} \rho_{\text{pol}} \int_{V_I} dV \int_{V_{II}} dV' \frac{3(\hat{\sigma}_1 \cdot \hat{r})(\hat{\sigma}_2 \cdot \hat{r}) - \hat{\sigma}_1 \cdot \hat{\sigma}_2}{r^3} = \sum_{n=\text{odd}}^{\infty} B_d^{(n)} \sin(2\pi n f_d t), \quad (3)$$

where  $V_I$  ( $V_{II}$ ) stands for the integration volume of the spin sensor (spin source),  $\mu_0$  is the vacuum permeability,  $\rho_{\text{pol}}$  is the polarized spin density of the spin source, and  $B_d^{(n)}$  is the  $n$ th Fourier coefficient of  $B_d$ . The frequency spectrum of  $B_d$  is shown in Fig. 2(b), including components at  $f_d$ ,  $3f_d$ ,  $5f_d$ , etc. We extracted the amplitude of the first-order harmonic  $B_d^{(1)}$  with a lock-in amplifier at  $f_d$ . As shown in Fig. 2(c), when MW II was on resonance,  $B_d^{(1)}$  was measured to be 6.41(9) nT. When MW II was off resonance, the result presented a zero signal. The polarized spin source density  $\rho_{\text{pol}}$  was then obtained to be  $(1.14 \pm 0.02) \times 10^{23} \text{ m}^{-3}$  when MW II was on resonance.

The experimental sequences to detect the SSVDIs are shown in Fig. 3(a), together with the time evolution of velocity  $v$  and corresponding effective magnetic field  $B_{\text{eff}}$ . Continuous application of MW II maintained the polarization of the spin source in a steady status, which enabled long-term stable searching. Since the spin source vibrates at a fixed frequency  $f_{\text{vib}} = 1.337 \text{ kHz}$ , the velocity of the spin source can be expressed as  $v(t) = 2\pi f_{\text{vib}} A \sin(2\pi n f_{\text{vib}} t)$ , where  $A = 36.7 \text{ nm}$  is the vibration amplitude. The effective magnetic field sensed by the ensemble-NV diamond magnetometer due to  $V_6$  is

$$B_{\text{eff}} = \frac{1}{V_I} \rho_{\text{pol}} \int_{V_I} dV \int_{V_{II}} dV' B_6 = \sum_{n=1}^{\infty} B_{\text{eff}}^{(n)} \sin(2\pi n f_{\text{vib}} t), \quad (4)$$

where  $B_{\text{eff}}^{(n)}$  is the  $n$ th Fourier coefficient of  $B_{\text{eff}}$ . Based on numerical simulations, the field strength primarily lies in the first-order harmonic component, as shown in Fig. 3(b) (see Supplemental Material for details [33]). The amplitude of the first-order harmonic  $B_{\text{eff}}^{(1)}$  was extracted by a lock-in amplifier with demodulation frequency being  $f_{\text{vib}}$ . After calibration of the phase  $\phi$  of the demodulation reference

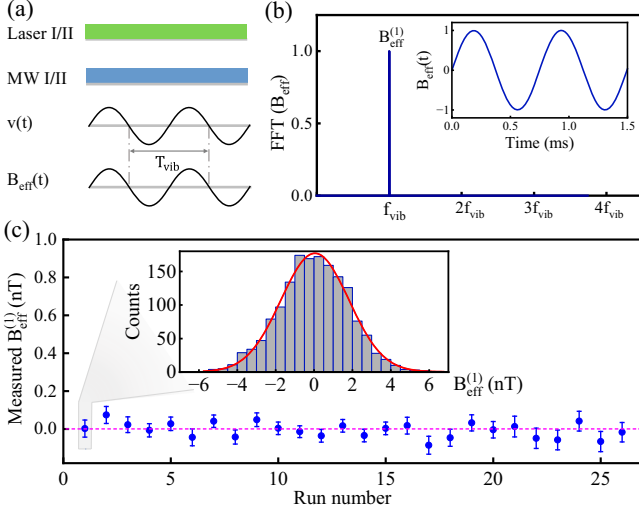


FIG. 3. Experimental searching for the SSVDis. (a) The experimental sequences and the time evolution of velocity  $v$  and the possible effective magnetic field  $B_{\text{eff}}$ .  $T_{\text{vib}} = 1/f_{\text{vib}}$ . (b) Fourier transformation spectrum of  $B_{\text{eff}}$ . Inset: calculated  $B_{\text{eff}}$  in time domain. (c) Experimental results of the measured effective magnetic field induced by SSVDis. Each point and its error bar represent the average and the standard error of 1 h dataset. The dashed magenta line marks the zero value of  $B_{\text{eff}}^{(1)}$ . The top inset shows the histogram of experimental results for the first 1 h dataset, in which the red solid line indicates a valid fit to the Gaussian distribution.

signal, the velocity-dependent signal  $B_{\text{eff}}^{(1)}$  and displacement-dependent signal correspond to the quadrature channel and in-phase channel of the lock-in amplifier, respectively. To mitigate the impact of magnetic dipole-dipole interactions, magnetic field shielding was usually employed in previous experiments [16,19], whereas in our study, it is unnecessary (see Supplemental Material for details [33]).

The total searching experiment was performed for 26 h to reduce statistical uncertainty. The mean value and the standard error of each dataset are shown in Fig. 3(c), where the fit in the inset indicates that each set of data follows a Gaussian distribution. With the overall 26-h data, the first-order amplitude of the effective magnetic field  $B_{\text{eff}}^{(1)}$  is determined to be  $(-2.8 \pm 7.8)$  pT with the reduced chi square  $\chi^2 = 0.82$ . The mean value of the measured effective field is smaller than its standard deviation, indicating no evidence of exotic SSVDis in this experiment. This sets new limits on the coupling coefficients corresponding to SSVDis.

Systematic errors are summarized in Table I, where we take  $\lambda = 1$  mm as an example. The main contributions come from the uncertainties of geometric parameters of the spin source, such as the radius of the polarized NV area and the thickness of the NV layer. The polarized spin density  $\rho_{\text{pol}}$  and its uncertainty were obtained by monitoring the magnetic dipole interaction over a long period. Other systematic errors include the uncertainty of the phase  $\phi$  of demodulation reference signal, the fluctuation of coefficient  $\eta$  between the magnetometer output voltage signal, and the sensed magnetic field. We also analyzed some other possible sources of systematic errors that are not listed due to their negligible effect, such as the effects of the moving surface charges and the demagnetization factor of the spin source (see Supplemental Material for details [33]). The overall systematic error was derived by assuming the systematic uncertainties independent of each other and combining all of them in quadrature. Therefore, we quote the final coupling coefficient as  $f_6 = (-0.27 \pm 0.76_{\text{stat}} \pm 0.06_{\text{sys}})$  for  $\lambda = 1$  mm, which determines  $|f_6| < 1.76$  at the 95% confidence level. By varying the force range and repeating a similar procedure, the constraints on coupling coefficients for the explored force ranges can be obtained.

TABLE I. Summary of systematic errors. The corrections to  $f_6$  and  $f_{14}$  with  $\lambda = 1$  mm are listed.

Parameter	Value	$\Delta f_6$	$\Delta f_{14}(10^{-10})$
Diameter $2R$	$104 \pm 1 \mu\text{m}$	$\pm 0.01$	$\pm 0.03$
Thickness $h_1$	$23 \pm 1 \mu\text{m}$	$\pm 0.01$	$\pm 0.01$
Thickness $h_2$	$23 \pm 1 \mu\text{m}$	$\pm 0.02$	$\pm 0.06$
Amplitude $A$	$36.7 \pm 0.5 \text{ nm}$	$\pm 0.01$	$\pm 0.02$
Distance $d$	$18.5 \pm 0.6 \mu\text{m}$	$\pm 0.01$	$\pm 0.01$
Phase $\phi$	$-6.7 \pm 4.4^\circ$	$\pm 0.01$	$-0.02$ $+0.01$
Deviation in x	$46 \pm 1 \mu\text{m}$	$-0.05$ $+0.04$	$\pm 0.01$
Relative angle	$54.0 \pm 0.4^\circ$	$\pm 0.01$	$\pm 0.01$
Coefficient $\eta$	$4.1 \pm 0.1 \text{ V/mT}$	$\pm 0.01$	$\pm 0.03$
Polarized density $\rho_{\text{pol}}$	$(1.14 \pm 0.02) \times 10^{23} \text{ m}^{-3}$	$\pm 0.01$	$\pm 0.02$
Final $f_6$	$-0.27$	$\pm 0.76$ (statistic) $\pm 0.06$ (systematic)	
Final $f_{14}$	$-1.36 \times 10^{-10}$		$\pm 3.80$ (statistic) $\pm 0.08$ (systematic)

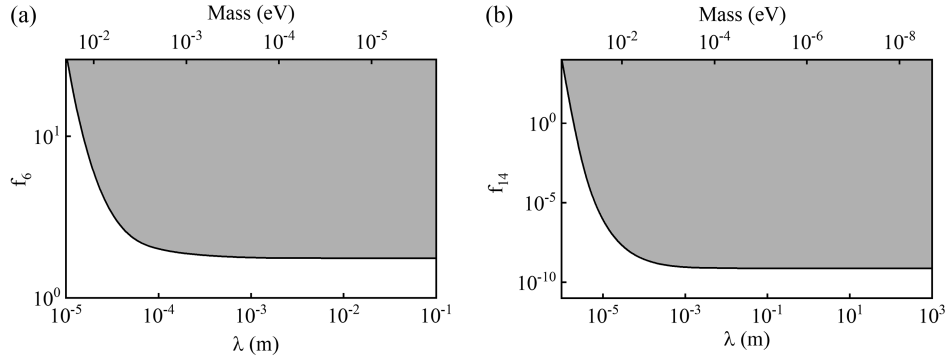


FIG. 4. (a) Experimental constraints on  $f_6$  between electrons as a function of the force range  $\lambda$  and the boson mass. The gray filled regions are excluded parameter spaces. The black line indicates upper limit on the coupling established by our experiment for the force range  $\lambda < 1$  cm. (b) Experimental constraints on  $f_{14}$  between electrons. Our work sets new constraints for the force range  $\lambda < 1$  km.

It is important to note that the geometric factors for different force ranges have been accounted for in the calculation.

Figure 4(a) shows the experimental constraints on  $f_6$  established by our work. For the force range from 1 cm to 1 km, the most stringent constraints were set by Ji *et al.* [16], in which a spin-exchange-relaxation-free comagnetometer was utilized to detect the possible effective magnetic field created by rotating SmCo<sub>5</sub> permanent magnets as electron spin sources. Our experiment is more sensitive to exotic interactions at micrometer scale and sets stringent limits in the force range from around 10  $\mu$ m to 1 cm.

Furthermore, our results can also be utilized to constrain another SSVDI between electrons:

$$V_{14} = f_{14} \frac{\hbar}{4\pi} [(\hat{\sigma}_1 \times \hat{\sigma}_2) \cdot \vec{v}] \left(\frac{1}{r}\right) e^{-r/\lambda}. \quad (5)$$

Only one preceding experiment has constrained directly on  $f_{14}$  using electron spins within the earth as the spin source [31]. However, that work has not provided constraints for  $\lambda < 1$  km, where fluctuations in the local polarized geoelectron density and potential local ferromagnetic interference will render the results unreliable at short ranges [30]. As shown in Fig. 4(b), our work explores the parameter space inaccessible for the geoelectron experiment, and offers new direct constraints on  $f_{14}$  in the force range of 1  $\mu$ m to 1 km.

In summary, we report a new experimental search of two types of SSVDis between polarized electrons. Using an NV ensemble as the spin sensor and another high-concentration NV ensemble as the spin source, we set new limits on  $V_6$  and  $V_{14}$  at the micrometer scale. We anticipate that further advances in experimentation will facilitate the search process in the future. To achieve higher polarized spin density, we can use high-power laser and microwave pulses to polarize the spin source. Moreover, using a silicon carbide heat spreader connected to the diamond can mitigate laser-induced thermal effect [40], and employing an infrared absorption readout method can effectively

improve the detection efficiency [41]. The application of the pulsed magnetic detection method is expected to achieve a better signal contrast. Therefore, the magnetic sensitivity of the ensemble-NV diamond magnetometer can be improved. We note that although other SSVDis like  $V_7$ ,  $V_{15}$ ,  $V_{16}$  vanish between two identical electrons because of commutative antisymmetry [12,13], these exotic interactions involving electron spins and polarized nucleons may still exist and allow detection utilizing the extension of our platform. With the development of spin-mechanical quantum chip technology, the exotic interactions can be investigated at shorter force range [42]. Overall, taking advantages of manipulation of the polarized spin states, NV ensembles have demonstrated a potential for searching exotic spin-spin interactions beyond the standard model.

This work was supported by NSFC (T2388102, 12150010, 12205290, 12261160569, 12261131497), the Innovation Program for Quantum Science and Technology (2021ZD0302200), the National Key R&D Program of China (Grant No. 2021YFC2203100). X.R. thanks the Youth Innovation Promotion Association of Chinese Academy of Sciences for the support. Y.F.C., Y.W., M.J., and Y.X. thank the Fundamental Research Funds for Central Universities. Y.F.C. is supported in part by CAS Young Interdisciplinary Innovation Team (JCTD-2022-20), 111 Project (B23042). M.J. is supported in part by China Postdoctoral Science Foundation (2022TQ0330). This work was partially carried out at the USTC Center for Micro and Nanoscale Research and Fabrication.

Y. H. and H. L. contributed equally to this work.

\*Corresponding author: jm2012@ustc.edu.cn

†Corresponding author: xrong@ustc.edu.cn

‡Corresponding author: djf@ustc.edu.cn

[1] D.F. Jackson Kimball, D. Budker, T.E. Chupp, A. A. Geraci, S. Kolkowitz, J. T. Singh, and A. O. Sushkov, *Phys. Rev. A* **108**, 010101 (2023).

- [2] R. D. Peccei and H. R. Quinn, *Phys. Rev. D* **16**, 1791 (1977).
- [3] S. Weinberg, *Phys. Rev. Lett.* **40**, 223 (1978).
- [4] F. Wilczek, *Phys. Rev. Lett.* **40**, 279 (1978).
- [5] P. W. Graham, D. E. Kaplan, and S. Rajendran, *Phys. Rev. Lett.* **115**, 221801 (2015).
- [6] J. E. Kim and G. Carosi, *Rev. Mod. Phys.* **82**, 557 (2010).
- [7] P. Svrcek and E. Witten, *J. High Energy Phys.* **06** (2006) 051.
- [8] F. Wilczek, *Phys. Rev. Lett.* **49**, 1549 (1982).
- [9] B. A. Dobrescu, *Phys. Rev. Lett.* **94**, 151802 (2005).
- [10] N. Okada, S. Okada, D. Raut, and Q. Shafi, *Phys. Lett. B* **810**, 135785 (2020).
- [11] J. E. Moody and F. Wilczek, *Phys. Rev. D* **30**, 130 (1984).
- [12] B. A. Dobrescu and I. Mocioiu, *J. High Energy Phys.* **11** (2006) 005.
- [13] P. Fadeev, Y. V. Stadnik, F. Ficek, M. G. Kozlov, V. V. Flambaum, and D. Budker, *Phys. Rev. A* **99**, 022113 (2019).
- [14] M. S. Safronova, D. Budker, D. DeMille, D. F. Jackson Kimball, A. Derevianko, and C. W. Clark, *Rev. Mod. Phys.* **90**, 025008 (2018).
- [15] S. Kotler, R. Ozeri, and D. F. Jackson Kimball, *Phys. Rev. Lett.* **115**, 081801 (2015).
- [16] W. Ji, Y. Chen, C. Fu, M. Ding, J. Fang, Z. Xiao, K. Wei, and H. Yan, *Phys. Rev. Lett.* **121**, 261803 (2018).
- [17] H. Su, Y. Wang, M. Jiang, W. Ji, P. Fadeev, D. Hu, X. Peng, and D. Budker, *Sci. Adv.* **7**, eabi9535 (2021).
- [18] Y. Wang, H. Su, M. Jiang, Y. Huang, Y. Qin, C. Guo, Z. Wang, D. Hu, W. Ji, P. Fadeev, X. Peng, and D. Budker, *Phys. Rev. Lett.* **129**, 051801 (2022).
- [19] Y. Wang, Y. Huang, C. Guo, M. Jiang, X. Kang, H. Su, Y. Qin, W. Ji, D. Hu, X. Peng, and D. Budker, *Sci. Adv.* **9**, eade0353 (2023).
- [20] J. Ding, J. Wang, X. Zhou, Y. Liu, K. Sun, A. O. Adeyeye, H. Fu, X. Ren, S. Li, P. Luo, Z. Lan, S. Yang, and J. Luo, *Phys. Rev. Lett.* **124**, 161801 (2020).
- [21] X. Rong, M. Jiao, J. Geng, B. Zhang, T. Xie, F. Shi, C. K. Duan, Y. F. Cai, and J. Du, *Phys. Rev. Lett.* **121**, 080402 (2018).
- [22] M. Jiao, M. Guo, X. Rong, Y. F. Cai, and J. Du, *Phys. Rev. Lett.* **127**, 010501 (2021).
- [23] H. Liang, M. Jiao, Y. Huang, P. Yu, X. Ye, Y. Wang, Y. Xie, Y.-F. Cai, X. Rong, and J. Du, *Natl. Sci. Rev.* **10**, nwac262 (2023).
- [24] D. Wu, H. Liang, M. Jiao, Y.-F. Cai, C.-K. Duan, Y. Wang, X. Rong, and J. Du, *Phys. Rev. Lett.* **131**, 071801 (2023).
- [25] B. R. Heckel, W. A. Terrano, and E. G. Adelberger, *Phys. Rev. Lett.* **111**, 151802 (2013).
- [26] W. A. Terrano, E. G. Adelberger, J. G. Lee, and B. R. Heckel, *Phys. Rev. Lett.* **115**, 201801 (2015).
- [27] P. Jain and S. Mandal, *Int. J. Mod. Phys. D* **15**, 2095 (2006).
- [28] A. Almasi, J. Lee, H. Winarto, M. Smiciklas, and M. V. Romalis, *Phys. Rev. Lett.* **125**, 201802 (2020).
- [29] F. Ficek, D. F. Jackson Kimball, M. G. Kozlov, N. Leefer, S. Pustelny, and D. Budker, *Phys. Rev. A* **95**, 032505 (2017).
- [30] L. Hunter, J. Gordon, S. Peck, D. Ang, and J.-F. Lin, *Science* **339**, 928 (2013).
- [31] L. R. Hunter and D. G. Ang, *Phys. Rev. Lett.* **112**, 091803 (2014).
- [32] P. Langacker, *Rev. Mod. Phys.* **81**, 1199 (2009).
- [33] See Supplemental Material at <http://link.aps.org/supplemental/10.1103/PhysRevLett.132.180801> for details of the experimental setup, polarized spin density measurement, numerical simulations of interactions between two ensemble NV centers, and systematic error analysis, which includes Refs. [34–36].
- [34] D. R. Glenn, D. B. Bucher, J. Lee, M. D. Lukin, H. Park, and R. L. Walsworth, *Nature (London)* **555**, 351 (2018).
- [35] P.-H. Chu, N. Ristoff, J. Smits, N. Jackson, Y. J. Kim, I. Savukov, and V. M. Acosta, *Phys. Rev. Res.* **4**, 023162 (2022).
- [36] N. A. Poklonski, A. A. Khomich, I. A. Svito, S. A. Vyrko, O. N. Poklonskaya, A. I. Kovalev, M. V. Kozlova, R. A. Khmelnitskii, and A. V. Khomich, *Appl. Sci.* **13**, 6221 (2023).
- [37] M. W. Doherty, N. B. Manson, P. Delaney, F. Jelezko, J. Wrachtrup, and L. C. L. Hollenberg, *Phys. Rep.* **528**, 1 (2013).
- [38] Y. Xie, H. Yu, Y. Zhu, X. Qin, X. Rong, C.-K. Duan, and J. Du, *Sci. Bull.* **66**, 127 (2021).
- [39] J. F. Barry, M. J. Turner, J. M. Schloss, D. R. Glenn, Y. Song, M. D. Lukin, H. Park, and R. L. Walsworth, *Proc. Natl. Acad. Sci. U.S.A.* **113**, 14133 (2016).
- [40] J. M. Schloss, J. F. Barry, M. J. Turner, and R. L. Walsworth, *Phys. Rev. Appl.* **10**, 034044 (2018).
- [41] G. Chatzidrosos, A. Wickenbrock, L. Bougas, N. Leefer, T. Wu, K. Jensen, Y. Dumeige, and D. Budker, *Phys. Rev. Appl.* **8**, 044019 (2017).
- [42] L. Wu, S. Lin, X. Kong, M. Wang, J. Zhou, C.-K. Duan, P. Huang, L. Zhang, and J. Du, *Proc. Natl. Acad. Sci. U.S.A.* **120**, e2302145120 (2023).